Magnetic anisotropy of Kondo semiconductor CeT_2Al_{10} (T = Ru,Os) in the ordered state

H. Tanida,[1] Y. Nonaka,[1] D. Tanaka,[1] M. Sera,[1] Y. Kawamura,[2] Y. Uwatoko,[2] T. Nishioka,[3] and M. Matsumura[3]
[1]*Department of ADSM, Hiroshima University, Higashi-Hiroshima 739-8530, Japan*
[2]*Institute for Solid State Physics, University of Tokyo, Kashiwa, Chiba 277-8581, Japan*
[3]*Graduate School of Integrates Arts and Science, Kochi University, Kochi 780-8520, Japan*
(Received 25 January 2012; published 17 May 2012)

We studied the applied magnetic field direction (θ) dependence of the magnetic and transport properties of CeT_2Al_{10} (T = Ru, Os) in the ab, bc, and ca planes focusing on the magnetic anisotropy in the ordered state. The magnetization of $NdOs_2Al_{10}$ was also studied as a reference of CeT_2Al_{10}. The results of $NdOs_2Al_{10}$ in the antiferromagnetic (AFM) state could be understood as a normal localized AFM compound. In CeT_2Al_{10}, the magnetic susceptibility in the ab, bc, and ca planes exhibits a smooth $\cos\theta$-like θ dependence both in the ordered state and the paramagnetic region. This suggests that the antiferromagnetic moment ($m_{\rm AFM}$) is not so strongly fixed along the c axis in the ordered phase, which indicates that the anisotropic AFM exchange interaction along the c axis is not strong and a coupling between the orbital moment of the Ce ion and the lattice is also small. The θ dependence of H^* in the bc and ca planes strongly supports the spin-flop transition from $m_{\rm AFM} \parallel c$ to $m_{\rm AFM} \parallel b$ at H^* for $H \parallel c$ unexpected from the smallest magnitude of the magnetic susceptibility along the b axis, which was recently proposed by our ^{27}Al NMR studies. From the θ dependence of H^* in the ca plane, we propose that the phase II observed in a high-field magnetization curve a little below the critical field to the paramagnetic region for $H \parallel a$ is the spin-flop phase B with $m_{\rm AFM} \parallel b$. H^* in $CeOs_2Al_{10}$ is about twice larger than that in $CeRu_2Al_{10}$, and when the temperature approaches to the transition temperature (T_0) from the low temperature, H^* of $CeOs_2Al_{10}$ exhibits the unusual increase, but that of $CeRu_2Al_{10}$ is reduced. As the origin of the different behavior of H^* in these two compounds, we propose that the relative weight of the singlet component against the AFM component in the ordered state close to T_0 and also the c-f hybridization along the b axis are larger in $CeOs_2Al_{10}$ than in $CeRu_2Al_{10}$. We conclude that the anisotropic c-f hybridization is the origin of the unusual magnetic anisotropy of CeT_2Al_{10} in the ordered state.

DOI: 10.1103/PhysRevB.85.205208 PACS number(s): 75.30.Gw, 71.27.+a

I. INTRODUCTION

Ce-based compounds have been studied extensively due to the appearance of the unexpected phenomena originating from the strong electron-electron correlation. The Kondo semiconductor is one of such interesting systems. The recently discovered Kondo semiconductor CeT_2Al_{10} (T = Ru, Os, Fe) has attracted much attention because of the unusual long-range order in $CeRu_2Al_{10}$ and $CeOs_2Al_{10}$.[1–31] These compounds are the first examples showing the magnetic order among the Kondo semiconductors, except the intermediate valence compound TmSe, which could be categorized into the Kondo semiconductor.[32] These compounds crystallize into the orthorhombic $YbFe_2Al_{10}$-type structure where the distance between the rare-earth ions is large and the interaction between them is expected to be weak.[1–3,5] The crystal structure of the present system is shown in Fig. 12. The shortest Ce-Ce distance is 5.26 Å and the second nearest one is 6.87 Å in $CeRu_2Al_{10}$. It is reported that the magnetic ordering temperatures in most of the Ce compounds in which the Ce-Ce distance exceeds 5 Å are below ∼2 K.[33] Among this series of compounds, CeT_2Al_{10} (T = Ru, Os, Fe) has been studied extensively. $CeRu_2Al_{10}$ and $CeOs_2Al_{10}$ exhibit the same type of unusual phase transition at high temperature of ∼30 K.[3,5] The magnetic susceptibility exhibits a large anisotropy of $\chi_a > \chi_c > \chi_b$ in the paramagnetic region, suggesting the large crystalline electric field (CEF) splitting in these compounds.[5,12,23] Here, χ_a, χ_b, and χ_c are the magnetic susceptibility along the a, b, and c axes, respectively. In $CeRu_2Al_{10}$, a Curie-Weiss behavior is observed in χ_a, indicating the valence of the Ce ion is close to 3+. On the other hand, in $CeFe_2Al_{10}$, the magnetic susceptibility is small and its temperature dependence is weak, which indicates that this compound is categorized into the valence fluctuation system.[4] Thus, the effect of the c-f hybridization is smallest in $CeRu_2Al_{10}$ and largest in $CeFe_2Al_{10}$. $CeOs_2Al_{10}$ is situated just between these two compounds. $CeRu_2Al_{10}$ and $CeOs_2Al_{10}$ exhibit the following characteristic magnetic properties. (1) The transition temperature (T_0) is very high regardless of a long distance between Ce ions. Even in GdT_2Al_{10} with a well-localized moment, T_N is 16 K.[5,21] (2) The antiferromagnetic (AFM) order is realized below T_0. The magnitude of the ordered moment (m_0) is small and the AFM moment ($m_{\rm AFM}$) is parallel to the c axis at $H = 0$, irrespective of the relation of $\chi_a > \chi_c$.[15,17,18] (3) Although m_0 in $CeRu_2Al_{10}$ is larger than that in $CeOs_2Al_{10}$, T_0 of $CeRu_2Al_{10}$ is lower than that of $CeOs_2Al_{10}$. The magnitude of m_0 is 0.42 and 0.29 μ_B/Ce in $CeRu_2Al_{10}$ with $T_0 = 27.3$ K and $CeOs_2Al_{10}$ with $T_0 = 28.7$ K, respectively.[5,18] This unusual relation between m_0 and T_0 strongly suggests that the origin of the long-range order is not the usual AFM exchange interaction and the important contribution of the c-f hybridization is suggested. (4) The magnetic susceptibility exhibits a decrease below T_0, independent of the crystal axes,[5,12] which is difficult to understand as a simple AFM order. There exists a large finite magnitude of χ_c at the lowest temperature regardless of $m_{\rm AFM} \parallel c$. We call this finite value of χ_c as a Van Vleck term, the origin of which is not known. (5) The specific heat (C) exhibits a sharp and large peak at T_0 and the magnetic entropy released at T_0 is about 0.7 Rln2 and 0.3 Rln2 in $CeRu_2Al_{10}$ and

$CeOs_2Al_{10}$, respectively.[5] This supports the trivalence of the Ce ion in the former and the closeness to the valence fluctuation regime in the latter. (6) C exhibits an exponential decrease with an excitation energy of ∼100 K below T_0 and χ_a also shows a similar exponential temperature dependence when a Van Vleck contribution at low temperatures is subtracted.[5] The inelastic neutron scattering experiments directly exhibited the existence of a large spin gap in the ordered state.[14,16] (7) T_0 of $CeRu_2Al_{10}$ is enhanced by applying pressure up to ∼2.5 GPa. At the same time, the physical properties become similar to those of $CeOs_2Al_{10}$, which is situated closer to the valence fluctuation region than $CeRu_2Al_{10}$. This indicates that the c-f hybridization is enhanced and m_0 is also reduced by pressure. The enhancement of T_0 by pressure regardless of the reduction of m_0 is quite strange. By further increase of pressure, T_0 is suppressed and suddenly disappears at ∼4 GPa and the physical properties become similar to those of $CeFe_2Al_{10}$, which is an intermediate valence compound.[5] Thus, it could be said that the unusual magnetic order in the present system takes place near the boundary between the localized and itinerant characters of the $4f$ electron. (8) The high-field magnetization curve exhibits a pronounced concave H dependence for $H \parallel a$ and a phase transition exists at $H_c^{\text{I-II}}$ a little below the critical field to the paramagnetic region H_c^p, although a spin canting magnetization process with $m_{\text{AFM}} \parallel c$ is realized for $H \parallel a$.[11,20] (9) The metamagneticlike transition exists at H^* in the magnetization curve for $H \parallel c$. H^* is ∼4 T and ∼7 T in $CeRu_2Al_{10}$ and $CeOs_2Al_{10}$, respectively.[12,13] The origin of this transition was not yet clarified. (10) The transport properties show the two-dimensional nature in the ca plane,[10] which might be associated with the anisotropic charge density distribution of $LaRu_2Al_{10}$, which indicates that the T-Al_{10} polyhedron is the fundamental component of the crystal and the rare-earth ion is located as nearly a free ion in the crevice constructed by the surrounding T-Al_{10} polyhedra.[24] The optical conductivity also shows such an anisotropic behavior.[25–27] (11) Although at high temperatures a Kondo semiconducting behavior is observed in the electrical resistivity, the ground state is a Fermi liquid, which is indicated by the observation of a Shubnikov–de Haas (SdH) oscillation.[19]

Although at the early stage, we proposed the possible long-range order with a singlet ground state below T_0,[7] soon after, Kambe and Khalyavin *et al.* reported that the AFM order with a small magnitude of $m_{\text{AFM}} \parallel c$ was realized below T_0 in $CeRu_2Al_{10}$.[9,15] Recently, Kondo *et al.* stressed the importance of the spin singlet in the ordered state based on the high-field magnetization of CeT_2Al_{10}.[20] The magnetization curve for $H \parallel a$ shows a pronounced concave H dependence in the ordered state. This concave H dependence of the magnetization is seen even at higher temperatures above T_0 up to ∼40 K in $CeOs_2Al_{10}$. This temperature of ∼40 K coincides with T_{max} where χ_a and χ_c exhibit a maximum. From these results, they concluded that the spin singlet accompanied with a large spin gap begins to be formed at T_{max} and coexists with the AFM order below T_0. Kondo *et al.* discussed that the largest c-f hybridization along the a axis could make a magnetization easy axis along the c axis, which leads to $m_{\text{AFM}} \parallel c$ at $H = 0$.

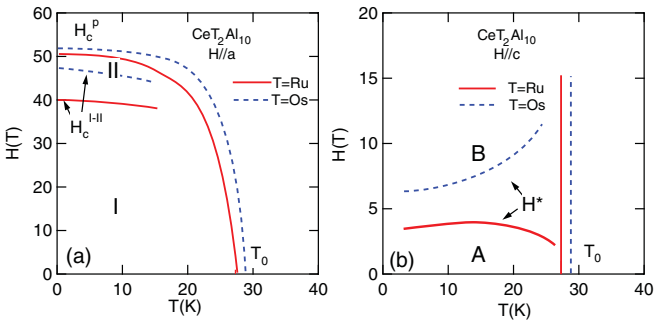

FIG. 1. (Color online) Schematic picture of the magnetic phase diagrams of $CeRu_2Al_{10}$ (red line) and $CeOs_2Al_{10}$ (blue dashed line) for (a) $H \parallel a$ cited from Refs. 11 and 20 and (b) $H \parallel c$ cited Refs. 12 and 13, respectively. Phase I for $H \parallel a$ is phase A for $H \parallel c$. Phase II for $H \parallel a$ is expected to be phase B for $H \parallel c$, and we conjecture that phase II for $H \parallel a$ is phase B for $H \parallel c$. See the discussion in details.

Quite recently, we reported the detailed results of ^{27}Al NMR in the ordered state of $CeRu_2Al_{10}$ using the single crystal.[30,31] The results at $H \sim 2.8$ T were explained consistently with the AFM order reported by the neutron diffraction results, i.e., $m_{\text{AFM}} \parallel c$ in zero magnetic field. The NMR results at $H \sim 4.4$ T above H^* for $H \parallel c$ indicate that m_{AFM} flips from the c to the b axis at H^*.[31] That is, in the spin-flip phase B, m_{AFM} is parallel to the b axis. This is quite strange because there exists a large anisotropy of $\chi_a > \chi_c > \chi_b$ in the paramagnetic region.

Here, we note the unusual characteristics of the magnetic phase diagram of CeT_2Al_{10}. Figures 1(a) and 1(b) show the schematic picture of the magnetic phase diagrams of $CeRu_2Al_{10}$ and $CeOs_2Al_{10}$ for $H \parallel a$ and c, respectively.[11–13,20] In the phase I for $H \parallel a$, a spin canting magnetization process with $m_{\text{AFM}} \parallel c$ is realized and this phase is expected to be continuously changed to the paramagnetic region at the critical field H_c^p. However, the other phase II exists a little below H_c^p. For $H \parallel c$, H^* exists at 4 ∼ 7 T. While T_0 is not affected by magnetic field up to 15 T in both compounds, H^* shows a largely different temperature dependence between two compounds. The magnitude of H^* of $CeOs_2Al_{10}$ is about twice larger than that of $CeRu_2Al_{10}$. Although in $CeRu_2Al_{10}$, H^* is suppressed when the temperature approaches to T_0 from the low-temperature side, H^* of $CeOs_2Al_{10}$ shows the unusual increase. The origin of the unusual temperature dependence of H^* in CeT_2Al_{10} has not yet been clarified.

In this paper, we performed the measurement of the magnetization, magnetostriction, electrical resistivity, and Hall resistivity of CeT_2Al_{10} to clarify the unusual magnetic anisotropy in the ordered state, which gives us the clue to understand the unusual AFM order in these compounds.

II. EXPERIMENT

The single crystals of CeT_2Al_{10} (T = Ru, Os) and $NdOs_2Al_{10}$ were prepared by an Al flux method. The magnetic susceptibility of CeT_2Al_{10} was measured by SQUID magnetometer. In the magnetic susceptibility of $CeOs_2Al_{10}$, the lowest magnetic field is 2 T for $H \parallel b$ and c. The magnetization at low temperatures was measured by an extraction method

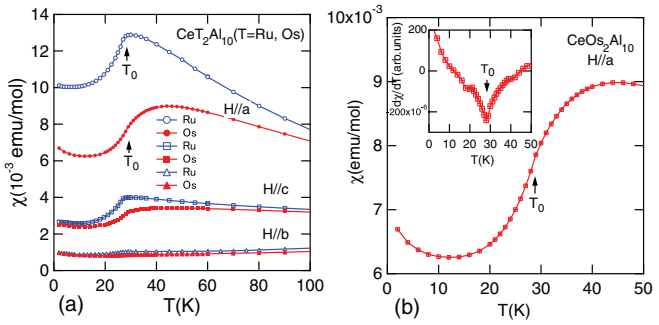

FIG. 2. (Color online) (a) Temperature dependence of magnetic susceptibility of CeT_2Al_{10} (T = Ru, Os) along the three crystal axes measured at $H = 1$ T. T_0 indicates the transition temperature of these compounds. (b) Temperature dependence of magnetic susceptibility of $CeOs_2Al_{10}$ along the a axis below 50 K. The inset shows the temperature dependence of $d\chi/dT$ in which T_0 is clearly recognized as a sharp dip.

up to $H = 10$ T. The magnetostriction was measured by a three-terminal capacitance method. The electrical resistivity and Hall resistivity were measured by a usual four-probe ac method and the θ dependence of the electrical resistivity was measured by using a homemade uniaxial rotator, where θ is the angle between the magnetic field and the crystal axis.

III. EXPERIMENTAL RESULTS

We performed the magnetization measurements of $NdOs_2Al_{10}$ at low temperatures as a reference compound of CeT_2Al_{10} showing the unusual properties. We found that the results of $NdOs_2Al_{10}$ could be explained as a normal localized magnetic compound. The results are shown in the Appendix, Sec. 1.

Here, we show the experimental results of CeT_2Al_{10}. The temperature (T) dependence of the magnetic susceptibility (χ) of CeT_2Al_{10} (T = Ru, Os) along the three crystal axes below $T = 100$ K is shown in Fig. 2(a). While χ_a and χ_c of $CeRu_2Al_{10}$ increase with decreasing temperature down to T_0 in the paramagnetic region, they exhibit a decrease toward T_0 below $T_{max} \sim 40$ K in $CeOs_2Al_{10}$. In $CeRu_2Al_{10}$, χ along all the crystal axes exhibits a clear kink at T_0 and a decrease below T_0. In $CeOs_2Al_{10}$, a clear kink is observed at T_0 for $H \parallel c$, but it is difficult to recognize for $H \parallel a$. While the anomaly is scarcely recognized even in the expanded scale in Fig. 2(b), in the T dependence of $d\chi/dT$, which is shown in the inset of Fig. 2(b), a sharp dip is seen at T_0. The upturn of χ below ~10 K is attributed to the Curie term from the magnetic impurity.

Figures 3(a) and 3(b) show the M-H and dM/dH-H curves of $CeRu_2Al_{10}$ at $T = 18$ K, respectively, where the applied magnetic field lies in the ca and bc planes. The definition of θ is shown in Fig. 13. In the ab plane, the magnetization increases in proportion to H independent of θ, while they are not shown in Fig. 3(a). The magnetization curve for $H \parallel c$ shows an anomaly at $H^* \sim 4$ T as was previously reported.[12] This is clearly seen as a maximum at ~3.9 T in the dM/dH-H curve. In the case of $\theta = 30°$ in the ca plane, H^* increases up to 4.5 T. In the case of $\theta = 60°$ and 90° in the ca plane, M is proportional to H up to 5 T, while they

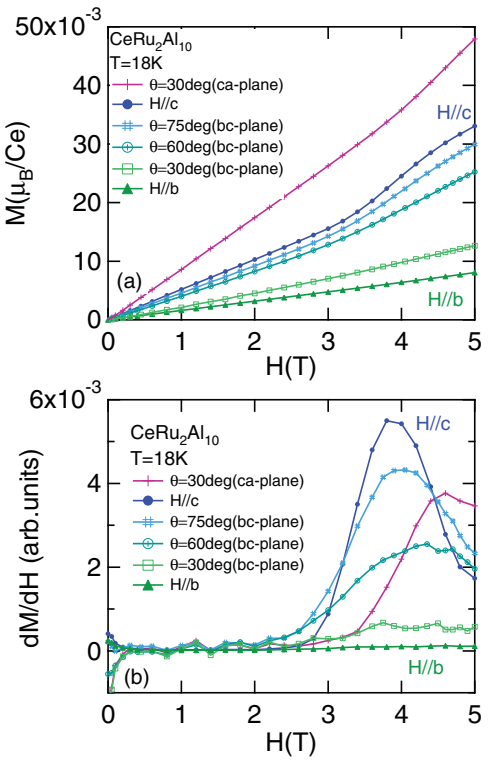

FIG. 3. (Color online) (a) Magnetization curve and (b) dM/dH-H curve of $CeRu_2Al_{10}$ at $T = 18$ K, where the magnetic field is rotated in the ca and bc planes. The definition of θ is shown in Fig. 13. The origin of the vertical axis in the figure (b) is shifted so as to be zero at $H = 0$ in each curve.

are not shown in Fig. 3(a). In the bc plane, when H is rotated from the c to the b axis, the anomaly at H^* is rapidly smeared out. As for the θ dependence, H^* increases when H is rotated from the c to the a axis, but is not so much changed when H is rotated from the c to b axis.

Figure 4 shows the T dependence of χ_c of CeT_2Al_{10} [(a) T = Ru, (b) T = Os)] below 50 K. In the paramagnetic region, χ_c of $CeRu_2Al_{10}$ shows an increase with decreasing temperature. A small maximum is seen at ~30 K. In $CeOs_2Al_{10}$, it decreases toward T_0 after showing a broad maximum at ~40 K. At low magnetic fields of 1 or 2 T, χ_c shows a rapid decrease below T_0 in both compounds. At $H = 5$ T, which is above H^* in $CeRu_2Al_{10}$, after showing a decrease below T_0, χ_c is nearly independent of temperature below $T \sim 15$ K. This T dependence of χ_c could be understood by $m_{AFM} \perp H$. In $CeOs_2Al_{10}$, $H = 7$ T is above H^* below ~17 K and below H^* above ~17 K. While the experimental result of χ_c at $H = 5$ and 7 T shows an increase below ~15 K, this is expected to originate from the Curie term from the magnetic impurity. The thin solid line exhibits the speculated intrinsic T dependence of χ_c in the ordered state after subtracting the Curie term from the magnetic impurity, although this is not exactly correct.

Figure 5 shows the T dependence of χ_b of $CeRu_2Al_{10}$ and $CeOs_2Al_{10}$ below 50 K. In $CeRu_2Al_{10}$, the results measured at $H = 1$ and 5 T are shown. In $CeOs_2Al_{10}$, those measured at $H = 2$ and 5 T are shown. The upturn below 15 ~ 20 K is attributed to the Curie term from the magnetic impurity. In the paramagnetic region, χ_b decreases with decreasing

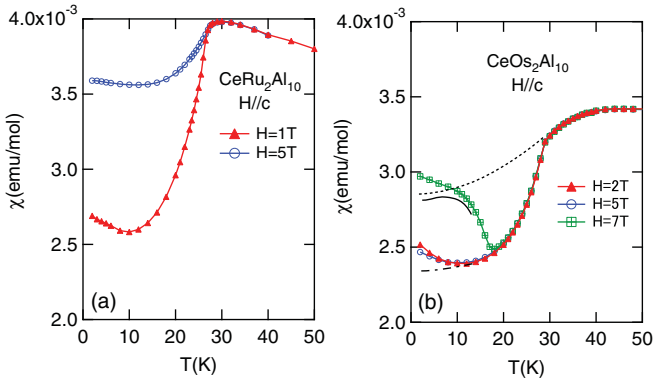

FIG. 4. (Color online) Temperature dependence of the magnetic susceptibility of CeT_2Al_{10} [(a) T = Ru, (b) T = Os] for $H \parallel c$. In (a), the applied magnetic field is 1 and 5 T. In (b), the applied magnetic field is 2, 5, and 7 T. The dotted line in (b) shows the expected temperature dependence of χ_c assuming the paramagnetic state continues to exist down to the lowest temperature. The dashed-dotted line in the figure (b) shows the expected temperature dependence of χ_c at $H = 5$ T without the Curie term from the magnetic impurity. The solid thin line in the figure (b) shows the speculated temperature dependence of χ_c at $H = 7$ T without a Curie term from the magnetic impurity. We note that these lines are not exactly drawn but the qualitative ones.

temperature after taking a broad maximum at ∼250 K in both compounds.[20] In $CeRu_2Al_{10}$, χ_b exhibits a very shallow minimum at ∼50 K and in $CeOs_2Al_{10}$ it continues to decrease down to T_0. Below T_0, χ_b of $CeRu_2Al_{10}$ shows a rapid decrease. In $CeOs_2Al_{10}$, a kink at T_0 is not pronounced. Thus, χ shows a decrease below T_0 independent of the applied magnetic field direction in both compounds, which is difficult to understand by a simple AFM order.

Figure 6 shows the T dependence of χ of $CeRu_2Al_{10}$ measured at $H = 1$ and 5 T. The magnetic field is rotated in the bc and ca planes. For $H \parallel a$ and $\theta = 60^\circ$ in the ca plane, χ measured at $H = 1$ T just coincides with that measured at $H = 5$ T apart from a Curie term at low temperatures. This indicates that the magnetization increases in proportion to H

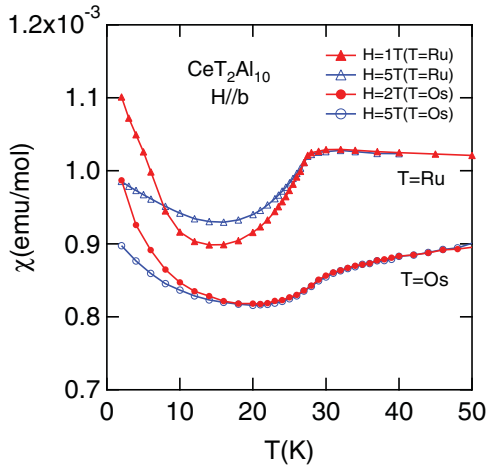

FIG. 5. (Color online) Temperature dependence of magnetic susceptibility of CeT_2Al_{10} (T = Ru, Os) for $H \parallel b$. The applied magnetic field is 1 and 5 T for T = Ru and 2 and 5 T for T = Os.

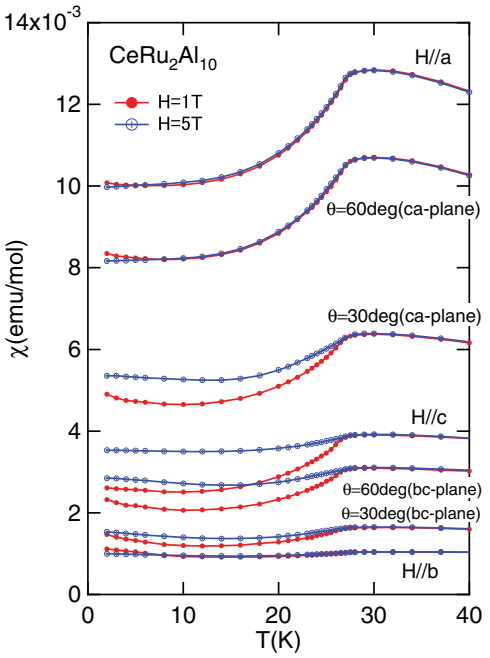

FIG. 6. (Color online) Temperature dependence of magnetic susceptibility of $CeRu_2Al_{10}$ measured at $H = 1$ and 5 T. The magnetic field is applied in the ca and bc planes. The definition of θ is shown in Fig. 13.

at least up to 5 T. For $\theta = 30^\circ$ in the ca plane, a large deviation between the T dependence of χ measured at $H = 1$ and 5 T is seen. This comes from the fact that 5 T does not belong to the low-field phase A below H^* but is located at $\sim H^*$. For $H \parallel c$, a difference between those measured at $H = 1$ and 5 T is largest. χ measured at $H = 5$ T is nearly independent of temperature below ∼20 K, which could be explained by $m_{\mathrm{AFM}} \perp H$ above H^*. For $\theta = 60^\circ$ in the bc plane, χ measured at $H = 1$ T shows a decrease below T_0, but that at $H = 5$ T is nearly independent of temperature below T_0. Also for $\theta = 30^\circ$ in the bc plane, the similar results are obtained, while a difference between χ measured at $H = 1$ and 5 T is smaller than that for $\theta = 60^\circ$. For $H \parallel b$, a difference between χ measured at $H = 1$ and 5 T is not recognized in this figure, but a small difference exists as is seen in Fig. 5.

Figures 7(a) and 7(b) show the θ dependence of χ in the ab, bc, and ca planes at $T = 10$ and 30 K and at $T = 18$ K, respectively. At $T = 30$ K, only the results measured at $H = 1$ T are shown because the magnetization curve is proportional to H. These are plotted from the results of the T dependence of χ in Fig. 6. χ in each plane shows a smooth $\cos\theta$-like θ dependence both below and above T_0. In the bc plane, χ measured at $H = 1$ T is smaller than that at $H = 5$ T in all the θ regions. Its difference is largest for $H \parallel c$ and decreases when H approaches to the b axis. In the ca plane, χ measured at $H = 1$ T coincides with χ measured at $H = 5$ T above $\theta = 60^\circ$. However, for $\theta < 30^\circ$, a clear difference appears. This comes from the fact that $H = 1$ T belongs to the low-field phase A below H^* and 5 T belongs to the high-field spin-flop phase B above H^*. The θ dependence of χ at $T = 18$ K is similar to that at $T = 10$ K. In the bc plane, a difference of χ between $H = 1$ and 5 T exists in all the θ regions, but in the

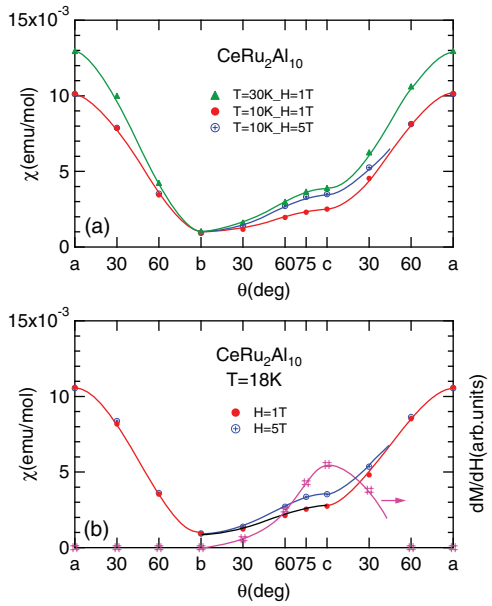

FIG. 7. (Color online) θ dependence of χ of $CeRu_2Al_{10}$ in the ab, bc, and ca planes at (a) $T = 10$ and 30 K and at (b) $T = 18$ K. At $T = 10$ and 18 K, the results measured χ at $H = 1$ and 5 T are shown. In the figure (b), a peak height of dM/dH shown in Fig. 3(b) is also drawn by the symbol #. The definition of θ is shown in Fig. 13.

ca plane, it does not exist at least for $\theta > 60^\circ$. In the ab plane, $H = 5$ T belongs to the low-field phase A independent of θ. χ measured at $H = 1$ T coincides with that at $H = 5$ T, although they are not shown here. This indicates that M increases in proportion to H at least up to 5 T in the ab plane.

Figure 8 shows the longitudinal magnetostriction ($\Delta l/l$) for $H \parallel a$, b, and c axes. $\Delta l/l$ along the b axis is almost independent of H up to 14.5 T. That along the a axis shows a large magnetic field dependence and a usual H^2 dependence up to 14.5 T. That along the c axis is almost independent of H up to H^*, but after showing a small elongation at H^*, increases in

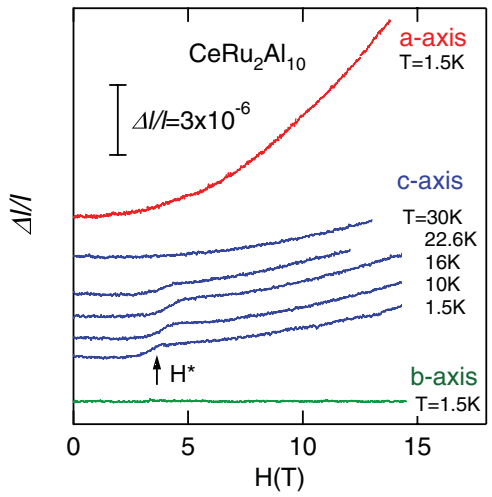

FIG. 8. (Color online) Longitudinal magnetostriction of $CeRu_2Al_{10}$ along the three crystal axes. Along the c axis, the results at several temperatures between 1.5 and 30 K are shown. The arrow for $H \parallel c$ indicates H^*.

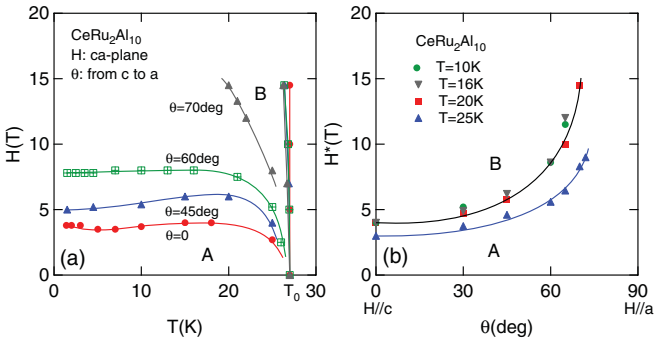

FIG. 9. (Color online) (a) Magnetic phase diagrams of $CeRu_2Al_{10}$ for several θ values in the ca plane. (b) θ dependence of θ^* in the ca plane. θ is the angle from the c axis in the ca plane.

proportion to H^2 above H^*. The magnitude of the elongation at H^* is very small and is less than 10^{-6}. We note that this small magnitude of the magnetostriction is much smaller than the shrinkage of the c axis below T_0, the order of which is 10^{-5} obtained in the thermal expansion.[7] The H^2 dependence is larger for $H \parallel a$ than for $H \parallel c$, which is expected from the larger magnitude of the magnetization for $H \parallel a$ than for $H \parallel c$.

From the results shown in the Appendix, Sec. 3, we obtained the magnetic phase diagrams of $CeRu_2Al_{10}$ shown in Figs. 9(a) and 9(b) for several θ values and the θ dependence of H^* at $T = 10$, 16, 20, and 25 K in the ca plane, respectively. The results at three temperatures of 10, 16, and 20 K are similar to each other apart from the results for $\theta = 70^\circ$, which originates from the parallel shift of the phase boundary between A and B. With increasing θ from the c axis, H^* increases and the increasing rate is much larger above $\theta = 60^\circ$ than below 45°. As is seen, in the result for $\theta = 70^\circ$ in Fig. 9(a), while the A-B phase boundary could be seen at the temperatures close to T_0, that below 20 K is not seen because it is far above 15 T.

Figures 10(a) and 10(b) show the T and H dependence of the Hall resistivity ρ_H, respectively. The electrical current flows along the b axis and the magnetic field is applied along the c axis. The Hall current flows in the ab plane. The T dependence shows a kink at T_0, which becomes clearer with increasing magnetic field. At higher magnetic fields, ρ_H exhibits a broad maximum at several Kelvins. As for the H dependence, ρ_H shows roughly an H-linear behavior above $\sim$10 K. At 15 and 20 K, a small anomaly is seen at H^*. At 1.5 K, an oscillation

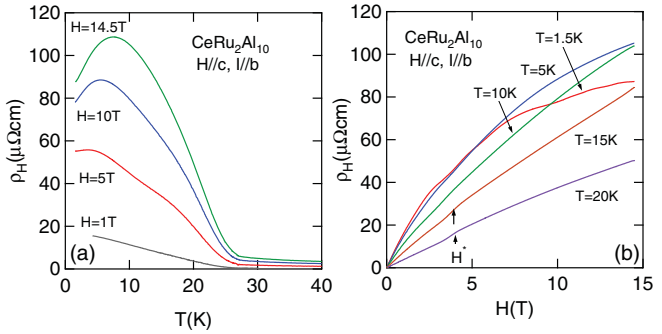

FIG. 10. (Color online) Hall resistivity of $CeRu_2Al_{10}$ measured under the magnetic field along the c axis. Hall current flows in the ab plane.

is observed. Although the periodicity of the oscillation is not simply proportional to $1/H$, this could be due to a quantum oscillation indicating the existence of the Fermi surface in the ground state. The SdH oscillation was observed in a high-field magnetoresistance.[19] A small anomaly at H^* indicates that the effect on the Fermi surface by the spin-flop transition at H^* is small.

IV. DISCUSSION

First, we discuss the magnetic anisotropy of $NdOs_2Al_{10}$. Previously, we reported the magnetic susceptibility, thermal expansion, and specific heat of NdT_2Al_{10}.[24,34] The results of the magnetic susceptibility and specific heat indicate a small CEF splitting in NdT_2Al_{10}. The overall CEF splitting is estimated to be about 200 K and the first excited doublet is expected to be located about 80 K above the CEF ground state. The small lattice distortion below T_N indicates a small coupling between the orbital moment of Nd ion and the lattice, which is consistent with the small CEF splitting. The existence of the first CEF excited state should be associated with a small χ_b in the paramagnetic region with a shoulder at $\sim$25 K and a small M_b at low temperatures. $m_{AFM} \parallel a$ expected from the T dependence of χ_a, χ_b, and χ_c below T_N is consistent with the largest magnitude of M_a. For $H \parallel a$, the magnetization curve shows not a spin-flop transition, but a direct transition from the AFM state with $m_{AFM} \parallel a$ to the paramagnetic region at H_c. This transition is that of the second order, and in the AFM state, the magnitude of m_{AFM} parallel to H is enhanced and that antiparallel to H is suppressed, which induces a continuous increase of the uniform magnetization along H. Such an increase of M takes place as the temperature is finite. At $T = 0$ K, the magnetization curve should show the first-order phase transition like a spin-flop transition below H_c. The smooth θ dependence of M at $T = 1.4$ K when the applied magnetic field is rotated in three planes and also a smooth θ dependence of H_c means that the magnetic anisotropy in the AFM ordered state is not so strong. When the magnetic field is rotated from the a axis in the bc and ca planes, the magnetic moment contains both the parallel and perpendicular components and their weight changes continuously. In a θ region close to the a axis, the parallel component is large and the perpendicular one is small. In a θ region close to the b and c axes, the former is small and the latter is large. The preliminary mean-field calculation assuming the isotropic AFM exchange interaction and the two-sublattice AFM magnet could reproduce the characteristic behaviors of the magnetization at $T \geqslant 1.4$ K quite well.[35] Below 1 K, a spin-flop transition to the AFM state with $m_{AFM} \parallel c$ is obtained below H_c by the mean-field calculation. Thus, the magnetic anisotropy of NdT_2Al_{10} is normally explained as a normal localized magnetic system.

Next, we discuss the coupling between the orbital moment of the Ce ion and the lattice in $CeRu_2Al_{10}$. The anomaly is observed at H^* in the longitudinal magnetostriction along the c axis. This should originate from the reorientation of m_{AFM} from the c axis. It is now known that at H^*, a spin-flop transition from $m_{AFM} \parallel c$ to $m_{AFM} \parallel b$ takes place from the results of our ^{27}Al NMR.[31] If the coupling between the orbital moment of the Ce ion and the lattice is strong, a large lattice distortion is expected to appear at H^*. However, the observed anomaly at H^* is very small. It is noted that in CeB_6 with $T_N = 2.3$ K and NdB_6 with $T_N = 8$ K, the magnitude of the lattice distortion below T_N is of the order of 10^{-5} and 10^{-4}, respectively.[36,37] These results indicate the small orbital-lattice coupling in $CeRu_2Al_{10}$. On the other hand, χ of CeT_2Al_{10} exhibits a large anisotropy at high temperatures. Generally, this leads to a large CEF splitting and a large orbital-lattice coupling. However, this is not consistent with the present results of the magnetostriction. Then, we expect that a large CEF splitting in CeT_2Al_{10} could not be ascribed to the usual Coulomb interaction, but the c-f hybridization plays an important role. The general concept that a small coupling between the orbital moment of the rare-earth ion and the lattice leads to a small CEF splitting is not applicable to CeT_2Al_{10} among the series of LnT_2Al_{10} (Ln = rare-earth element). The relation between the small orbital-lattice coupling and the large CEF splitting should be examined in the future.

Now, we discuss the θ dependence of χ of $CeRu_2Al_{10}$ in the ab, bc, and ca planes. Both below and above T_0, χ shows a smooth $\cos\theta$-like θ dependence in all the planes as shown in Fig. 7. A smooth θ dependence of χ below T_0 indicates that there does not exist a large magnetic anisotropy which fixes the magnetic moment tightly along a specific crystal axis in the ordered state. This is consistent with a small lattice distortion at H^*, and also suggests that although the anisotropic AFM exchange interaction along the c axis should be largest considering $m_{AFM} \parallel c$ at $H = 0$, it is not strong enough to fix m_{AFM} along the c axis tightly. In the Appendix, Sec. 4, we discuss the relation between the θ dependence of H^* and the direction of m_{AFM} in the bc and ca planes and conclude that at H^*, a spin-flop transition from $m_{AFM} \parallel c$ to $m_{AFM} \parallel b$ takes place. The fact that $m_{AFM} \parallel b$ is realized above H^* around $H \parallel c$ is unexpected from the relation of $\chi_a > \chi_c > \chi_b$ in the paramagnetic region. This indicates that a quite unusual magnetic anisotropy exists in CeT_2Al_{10}, which is different from the normal case in NdT_2Al_{10}. We propose the importance of the anisotropic c-f hybridization as the origin of the unusual magnetic anisotropy in CeT_2Al_{10}. Recently, from the high-field magnetization curves of CeT_2Al_{10}, Kondo *et al.* concluded that the AFM order is accompanied with a Kondo singlet character, and as the origin of $m_{AFM} \parallel c$ at $H = 0$, they proposed that the largest c-f hybridization along the a axis makes it difficult for the magnetic moment to be induced along the a axis and forces m_{AFM} parallel to the c axis in place of the a axis expected from the relation of $\chi_a > \chi_c$ in the paramagnetic region.[20] The present conclusion of $m_{AFM} \parallel b$ above H^* for $H \parallel c$ could be also explained by the strong c-f hybridization along the a axis. That is, m_{AFM} is difficult to align along the a axis and could rotate only in the bc plane. The reason why $m_{AFM} \parallel c$ is realized at $H = 0$ is that M_b is extremely small, but above H^*, the Zeeman energy gain by $\chi_\perp$ is dominant, which leads to $m_{AFM} \parallel b$.

Figures 11(a) and 11(b) show the speculated θ dependence of H^* in the ca plane and H_c^p together with H^* in the ab, bc, and ca planes, respectively. Considering that there exists H^* for $H \parallel c$ at $\sim$4 T and $H^{\text{I-II}}$ for $H \parallel a$ at $\sim$40 T and a strong increase of H^* for $\theta > 70^\circ$, H^* is expected to be continued to $H^{\text{I-II}}$ for $H \parallel a$ as shown by a dashed line in Fig. 11(a). Thus, we conjecture that the phase II for $H \parallel a$ is the phase B for $H \parallel c$.[12,20] The θ dependence of H_c^p is expected to be similar to

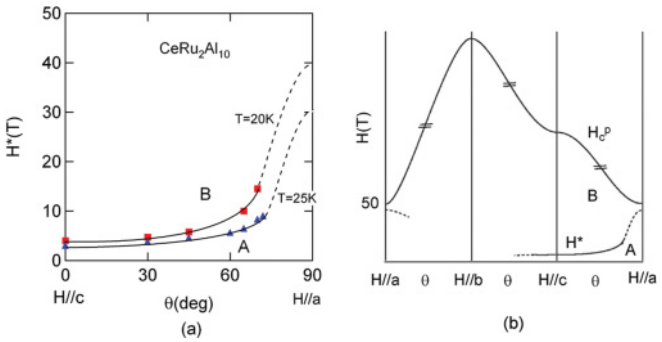

FIG. 11. (Color online) Schematic picture of the speculated θ dependence of (a) H^* in the ca plane in $CeRu_2Al_{10}$ and (b) H_c^pc and $H^{\mid *}$ in the ab, bc, and ca planes. Around $H \parallel b$, no transition except H_c^p is expected.

that of $NdOs_2Al_{10}$ shown in Figs. 14(a2)–14(c2) apart from the different magnitude of H_c. The difference between CeT_2Al_{10} and NdT_2Al_{10} is the existence or nonexistence of the transition at H^*. For $H \parallel a$, a spin canting magnetization process with $m_{AFM} \parallel c$ should be realized at least up to $H_c^{I\text{-}II}$. In both phases of A and B, the spin configuration with $m_{AFM} \perp H$ is expected to be realized. In the A phase, $m_{AFM} \parallel c$ is realized and in the B phase, we conjecture that $m_{AFM} \parallel b$ is realized. The high-field magnetization for $H \parallel a$, the concave H dependence is seen in the A phase and a rapid increase in the B phase. This suggests that it is difficult to induce the magnetization along the a axis when m_{AFM} is located in the ca plane and easily induced when m_{AFM} is located in the ab plane. We propose that this may be because the spin-singlet component is larger in the ca plane than in the ab plane. The transition to the B phase at 40 T may be ascribed to the dominant contribution of the Zeeman interaction.

Finally, we discuss the different T dependence of H^* in the magnetic phase diagram for $H \parallel c$ between $CeRu_2Al_{10}$ and $CeOs_2Al_{10}$ shown in Fig. 1(b). The magnitude of H^* reflects the strength of the magnetic anisotropy along the c axis. Then, a roughly twice larger H^* in $CeOs_2Al_{10}$ than in $CeRu_2Al_{10}$ means that the magnetic anisotropy is larger in $CeOs_2Al_{10}$ than in $CeRu_2Al_{10}$. However, this contradicts with the fact that the Ce ion in $CeOs_2Al_{10}$ is closer to the valence fluctuation regime than in $CeRu_2Al_{10}$, and the ordered moment is smaller in the former than in the latter. Furthermore, the T dependence of H^* is different between these two compounds. First, we consider the reason why H^* is higher in $CeOs_2Al_{10}$ than in $CeRu_2Al_{10}$. χ_b exhibits a continuous decrease with decreasing temperature down to T_0 in the paramagnetic region in $CeOs_2Al_{10}$, different from nearly a constant χ_b below $\sim$50 K in $CeRu_2Al_{10}$ as shown in Figs. 2 and 5. This indicates that in $CeOs_2Al_{10}$, the c-f hybridization effect exists not only in the ca plane, but along the b axis from the high-temperature region above T_0 and the latter makes m_{AFM} difficult to be aligned along the b axis. This could lead to the higher H^* in $CeOs_2Al_{10}$ than in $CeRu_2Al_{10}$. The magnitude of H^* might be determined by the competition between the three interactions, i.e., the c-f hybridization, AFM exchange, and Zeeman interactions. As the origin of the different T dependence of H^* in CeT_2Al_{10}, we propose the following explanation. There exists the apparent difference in the T dependence of χ_c between $CeRu_2Al_{10}$ and $CeOs_2Al_{10}$. In the former, χ_c increases with decreasing temperature, but in the latter, a decrease of χ_c exists already below $T_{max} \sim 40$ K. Kondo *et al.* ascribed the origin of this decrease to the spin-singlet formation, which begins to appear below T_{max}.[20] Then, it is natural to ascribe the origin of the unusual T dependence of H^* in $CeOs_2Al_{10}$ to the spin singlet, which appears below T_{max}. The weight of the singlet component below T_0 is larger in $CeOs_2Al_{10}$ than in $CeRu_2Al_{10}$, at least around T_0. The ratio between the singlet component and the AFM component is expected to change with temperature. In $CeOs_2Al_{10}$, at T_0, the singlet component already grows up because it appears below T_{max}. Then, it is difficult to induce the magnetic moment along the magnetic field, which makes H^* higher. When the temperature is lowered enough below T_0, the relative weight of the AFM component increases. This leads to a lower H^* at low temperatures than that at high temperatures. Thus, the unusual T dependence of H^* of $CeOs_2Al_{10}$ could be explained by the existence of the singlet formed below T_{max}. On the other hand, in $CeRu_2Al_{10}$, the singlet and the AFM component appear nearly at the same time at T_0, and the nearly same T dependence of the singlet and AFM components is expected below T_0. This does not induce the unusual T dependence of H^* as in $CeOs_2Al_{10}$. We conjecture that when the pressure is applied to $CeRu_2Al_{10}$, H^* is increased and the T dependence of H^* of this compound around T_0 becomes similar to that of $CeOs_2Al_{10}$.

V. SUMMARY

We studied the applied magnetic field direction (θ) dependence of the magnetic and transport properties of CeT_2Al_{10} (T = Ru, Os) in the ab, bc, and ca planes focusing on the magnetic anisotropy in the ordered state and also studied the magnetization of $NdOs_2Al_{10}$ as a reference of CeT_2Al_{10}. In $NdOs_2Al_{10}$, the easy magnetization axis in the AFM ordered phase is along the a axis, which is consistent with the relation of $\chi_a > \chi_c > \chi_b$ and the θ dependence of M and H_c in all the planes shows a continuous $\cos\theta$-like behavior. These results of $NdOs_2Al_{10}$ could be understood as a well-localized system with a normal magnetic anisotropy in the AFM state. In CeT_2Al_{10}, the magnetic susceptibility in the ab, bc, and ca planes exhibits a smooth $\cos\theta$-like θ dependence both in the ordered state and in the paramagnetic region. This indicates that m_{AFM} at $H = 0$ is not tightly fixed along the c axis by the anisotropic AFM exchange interaction along the c axis and also a coupling between the orbital moment of the Ce ion and the lattice is small, which is supported by a small anomaly of the magnetostriction at H^*. The θ dependence of $H^* \sim 4$ T of $CeRu_2Al_{10}$ in the bc and ca planes strongly supports the unexpected occurrence of a spin-flop transition from $M_{AFM} \parallel c$ to b at H^*, which was recently proposed by our ^{27}Al NMR studies. From the θ dependence of H^* in the ca plane, which increases rapidly for $\theta > 70^\circ$, we propose that the phase II observed in a high-field magnetization a little below H_c^p for $H \parallel a$ is the spin-flop phase B with $m_{AFM} \parallel b$ for $H \parallel c$. H^* in $CeOs_2Al_{10}$ is about twice larger than that in $CeRu_2Al_{10}$. In $CeOs_2Al_{10}$, H^* increases when the temperature approaches to T_0 from the low-temperature side and in $CeRu_2Al_{10}$, it is suppressed. As the origin of the different behavior of H^* in these two compounds, we propose that the relative weight

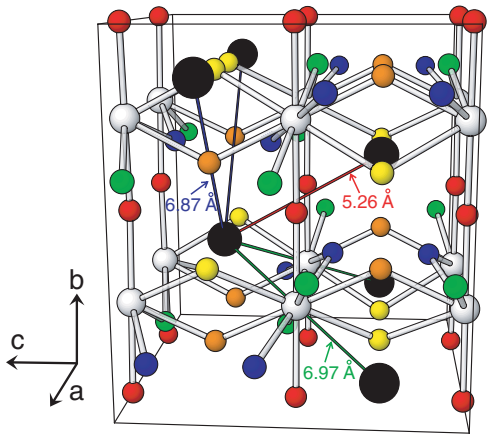

FIG. 12. (Color online) Crystal structure of LnT_2Al_{10}. Large closed circle and white circle mean Ln and T atoms, respectively. Small five circles (orange, yellow, blue, green, and red) mean Al1, Al2, Al3, Al4, and Al5 atoms, respectively. The distances between two Ce atoms for several bonds for $CeRu_2Al_{10}$ are shown in the figure.

of the singlet component against the AFM component in the ordered state close to T_0 and also the c-f hybridization along the b axis are larger in $CeOs_2Al_{10}$ than in $CeRu_2Al_{10}$. We conclude that the anisotropic c-f hybridization is highly associated with the origin of the unusual magnetic anisotropy in CeT_2Al_{10}.

APPENDIX

1. Crystal structure of LnT_2Al_{10}

The crystal structure of LnT_2A_{10} is shown in Fig. 12. The T and nearest five Al atoms are connected by tubes because these bonds are stronger than the others.[24] The distances between two Ce atoms for several bonds are shown in the figure. The shortest distance is 5.26 Å, which forms a zigzag chain along the c axis in the bc plane.

2. Magnetization of NdT_2Al_{10} at low temperatures

Figures 13(a)–13(c) show the magnetization curve of $NdOs_2Al_{10}$ at $T = 1.4$ K, where the magnetic field is rotated in the a, b, and c axes, respectively. The definition of θ is shown in Fig. 13. In the ab, bc, and ca planes, θ is the angle between the magnetic field and the ab, bc, and ca planes, respectively. The magnetization curves, the temperature (T) dependence of the magnetic susceptibilities, and magnetic phase diagrams along the three crystal axes were already reported in our previous paper and the Néel temperature T_N is 2.2 K.[24] The concave H dependence is observed for $H \parallel a$ and the H-linear behavior is observed for $H \parallel b$ and c. From these results and also the T dependence of the magnetic susceptibilities along the three crystal axes, the AFM order with $m_{AFM} \parallel a$ is expected to be realized. The magnetization for $H \parallel a$ (M_a) shows a concave H dependence up to $H_c = 2.2$ T and shows a shoulder at $H \sim 4$ T and a saturated behavior above 5 T. Here, H_c is a critical field from the AFM state to the paramagnetic region. With increasing θ in the ca plane, the concave H dependence below H_c becomes less pronounced and H_c increases. For $H \parallel c$, M_c shows an H-linear behavior up to

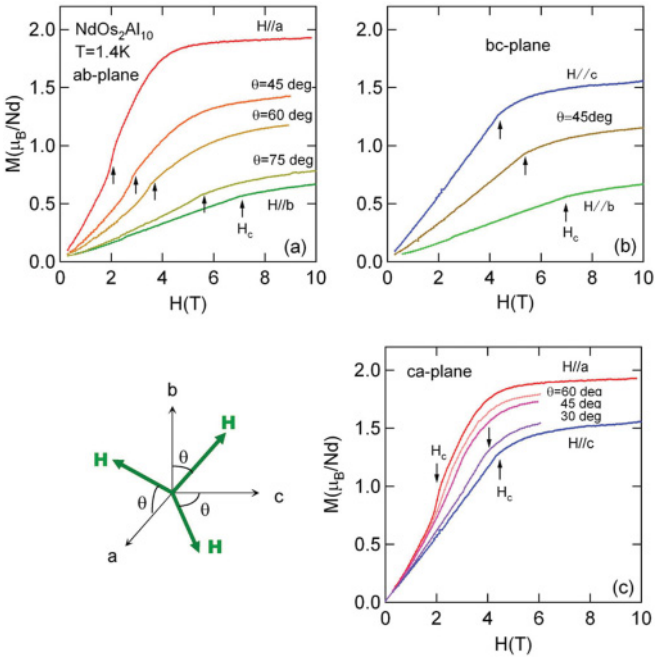

FIG. 13. (Color online) Magnetization curve of $NdOs_2Al_{10}$ at $T = 1.4$ K in (a) ab plane, (b) bc plane, and (c) ca plane. The θ is the angle between the applied magnetic field and the crystal axis in each plane. The arrow indicates the transition field to the paramagnetic region H_c.

$H_c = 4.3$ T, and above 6 T, a saturated behavior is observed. The magnetization curve does not show any discontinuous change as a function of θ. In the bc plane, all the results show an H-linear behavior up to H_c. This indicates that the spin canting magnetization process is always realized in the bc plane, which is expected from $m_{AFM} \parallel a$ in the AFM magnetic ordered state. In the ab and ca planes, the concave H dependence becomes less pronounced and H_c increases with increasing θ. The variation accompanied with an increase of θ is continuous.

Figures 14(a1)–14(c1) show the the θ dependence of M at $H = 7$ T in the ab, bc, and ca planes, respectively. The results at $H = 7$ T belong to the paramagnetic region. We note that in the ca plane, the values extrapolated to $H = 7$ T from the low-field results for $\theta = 30$, 45, and 60° because the measurements were performed only up to 6 T. In all the planes, M shows a smooth continuous θ dependence as expected in the paramagnetic region. Figures 14(a2)–14(c2) show the θ dependence of H_c in the ab, bc, and ca planes, respectively. H_c also shows a smooth continuous θ dependence in all the planes. This means that the AFM state with $m_{AFM} \parallel a$ changes continuously to the spin canting state with $m_{AFM} \parallel a$ for $H \parallel b$ and c.

3. θ dependence of the magnetoresistance of $CeRu_2Al_{10}$ in the ca and bc planes

Figures 15(a)–15(d) show the magnetoresistance of $CeRu_2Al_{10}$ measured at various θ values at $T = 10$, 16, 20, and 25 K, respectively. It is normalized by ρ at $H = 0$. The electrical current flows along the a axis and the magnetic field is rotated in the ca plane. θ is the angle from the c axis in the ca plane, as is shown in the inset of Fig. 15(d). The anomaly at H^*

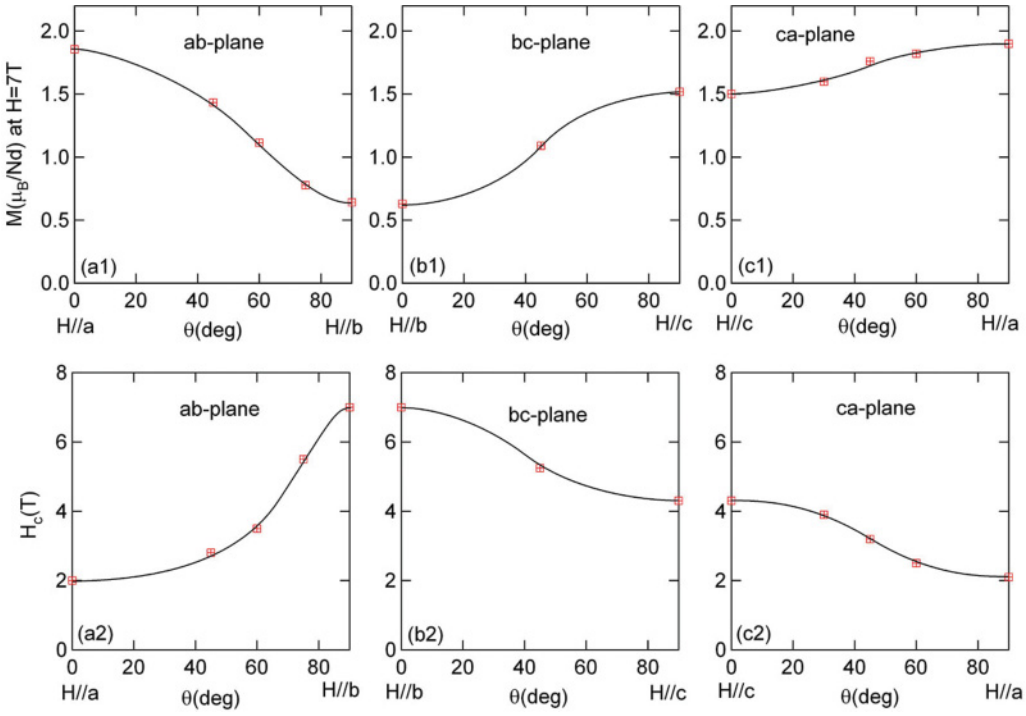

FIG. 14. (Color online) The θ dependence of (a) the magnetization at $H = 7$ T and (b) the critical field (H_c) to the paramagnetic region of $NdOs_2Al_{10}$ in the *ab*, *bc*, and *ca* planes at $T = 1.4$ K. The definition of θ is shown in Fig. 13. For the *ca* plane, the extrapolated values which are obtained from the low-field data up to 6 T in Fig. 13(c) are plotted. The solid lines are the guide to the eyes.

at low temperatures below 10 K is less pronounced than that above 15 K. For $\theta = 30^\circ$, a discontinuous change is observed at $H^* \sim 5$ T. With increasing the θ value, the anomaly of ρ at H^* becomes broader and H^* increases. It is difficult to recognize for $\theta > 70^\circ$. However, at $T = 25$ K, H^* is seen even for $\theta = 70^\circ$ because 25 K is close to T_0.

Figures 16(a) and 16(b) show the θ dependence of the transverse magnetoresistance of $CeRu_2Al_{10}$ at $T = 30$ and 20 K, respectively. The magnetic field is rotated in the *ca* plane and the electrical resistivity is normalized by the value for $\theta = 90^\circ$. At each temperature, the measurements were performed at $H = 5$, 8, and 14.5 T. The electrical current flows along the *b* axis and the magnetic field is applied in the

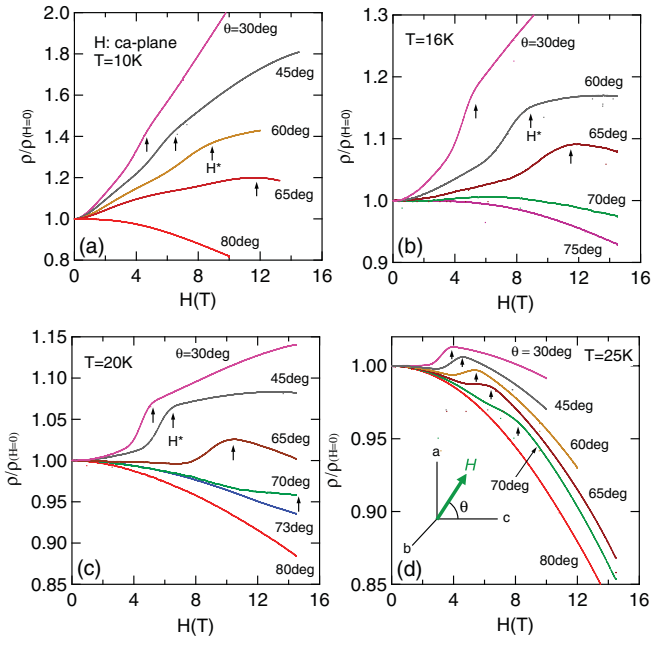

FIG. 15. (Color online) Magnetoresistance of $CeRu_2Al_{10}$ at (a) $T = 10$ K, (b) 16 K, (c) 20 K, and (d) 25 K measured under the various magnetic field directions in the *ca* plane. ρ in magnetic field is normalized by ρ at $H = 0$. The electrical current flows along the *a* axis. θ is the angle from the *c* axis in the *ca* plane as shown in Fig. 15(d). The arrow indicates the transition at H^*.

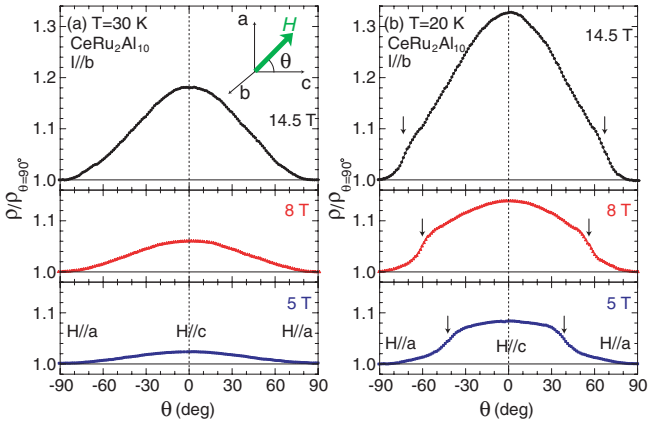

FIG. 16. (Color online) θ dependence of the transverse magnetoresistance of $CeRu_2Al_{10}$ in the *ca* plane at (a) $T = 30$ K and (b) 20 K. In both cases, the measurements were performed in the magnetic fields of 5, 8, and 14.5 T. The electrical current flows along the *b* axis. θ is the angle from the *c* axis in the *ca* plane. The arrow in the figure (b) corresponds to the transition between A and B phases.

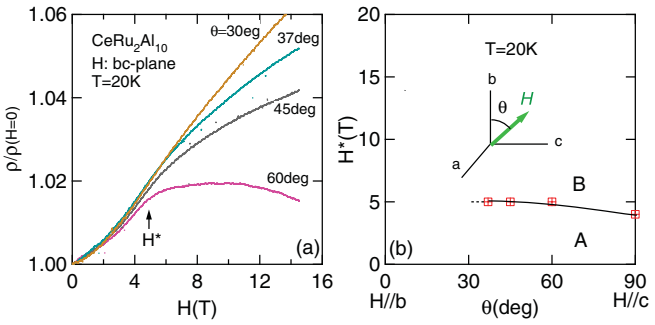

FIG. 17. (Color online) (a) Magnetoresistance of $CeRu_2Al_{10}$ at $T = 20$ K at various magnetic field directions. The electrical current flows along the c axis. θ is the angle from the b axis in the bc plane. (b) θ dependence of H^* in the bc plane.

ca plane. At $T = 30$ K in the paramagnetic region, ρ shows a $\cos\theta$-like θ dependence and its amplitude is larger at higher magnetic fields as usual. This is consistent with the results of the magnetic susceptibility shown in Fig. 2(a). At $T = 20$ K, the discontinuous anomaly is seen at the angle denoted by an arrow. This corresponds to the discontinuous change of ρ at H^* shown in Fig. 15. We call this angle as θ^*. θ^* increases with increasing magnetic field. At $H = 14.5$ T, θ^* is 70°, which is consistent with the results in Fig. 15. The θ dependence of ρ for $\theta < \theta^*$ is small at $H = 5$ T and pronounced at $H = 14.5$ T.

Figure 17(a) shows the magnetoresistance of $CeRu_2Al_{10}$ at $T = 20$ K. The electrical current flows along the c axis and the magnetic field is rotated in the bc plane. θ is the angle from the b axis in the bc plane. The results are very different from those in the ca plane. The anomaly at H^* is rapidly smeared out with decreasing θ from $H \parallel c$. For $\theta = 45°$, a discontinuous change is not clearly seen at H^*, while it is seen for $\theta = 60°$. The anomaly at H^* is rapidly smeared out and is not seen at $\theta = 60°$. Figure 17(b) shows the θ dependence of H^* at $T = 20$ K, which is very different from that in the ca plane.

4. Spin-flop transition at H^* in CeT_2Al_{10}

Here, we discuss that the θ dependence of χ and ρ are not consistent with a spin-flop transition from $m_{\rm AFM} \parallel c$ to $m_{\rm AFM} \parallel a$, but are consistent with that from $m_{\rm AFM} \parallel c$ to $m_{\rm AFM} \parallel b$. This indicates the existence of a quite unusual magnetic anisotropy in CeT_2Al_{10}. This is very different from the normal magnetic anisotropy in NdT_2Al_{10}. When the spin-flop transition takes place at H^*, two kinds of the configuration of $m_{\rm AFM}$ could be considered above H^*. One is that $m_{\rm AFM} \parallel a$ and the other is $m_{\rm AFM} \parallel b$ above H^*, which are shown in the cases (I) and (II) in Fig. 18, respectively. When H is rotated in the ab plane, the spin canting magnetization process with $m_{\rm AFM} \parallel c$ is expected to be always realized independent of θ from the fact that $m_{\rm AFM} \parallel c$ is realized at low magnetic fields for $H \parallel a$ and b. This leads to no anomaly in the θ dependence of χ and ρ in the ab plane at low magnetic fields, although they are not shown in this paper. First, we consider the case (I). This case is expected from the relation of $\chi_a > \chi_c > \chi_b$ in the paramagnetic region. For $H \parallel a$ and b, the spin canting magnetization process with $m_{\rm AFM} \parallel c$ is realized. Here, we consider the case where H is rotated in the ca plane above H^*, which is shown in Fig. 18(a). In this case, $m_{\rm AFM}$ is expected to be always perpendicular to H

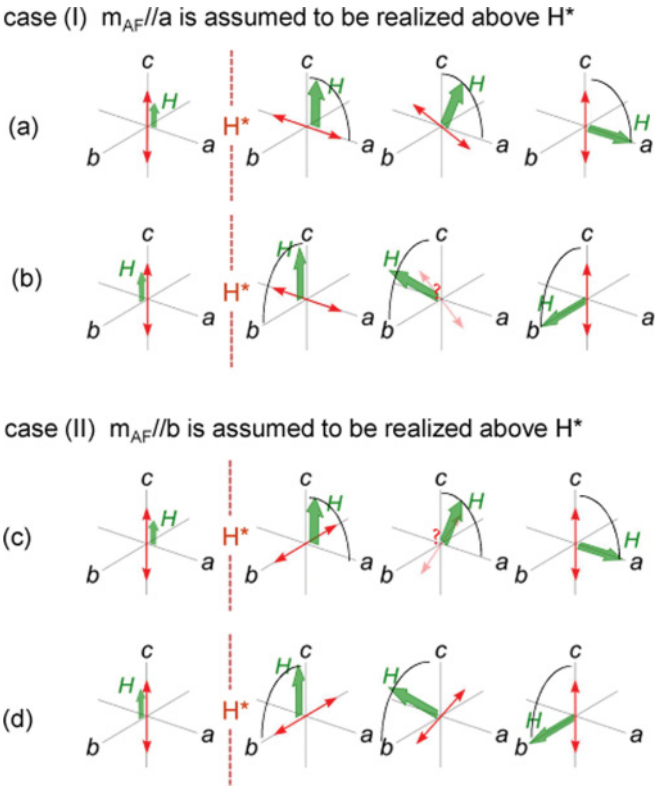

FIG. 18. (Color online) Schematic pictures of $m_{\rm AFM}$ when H is rotated in the (a) ca and (b) bc planes, respectively. Only the AFM magnetic components are shown by the antiparallel arrows and the uniform component along the magnetic field is not shown. The left picture is for $H < H^*$ and the right three ones are for $H > H^*$. The configuration for the intermediate magnetic field direction in the bc plane, which is shown in the middle of figure (b) for $H > H^*$, is unphysical if $m_{\rm AFM}$ is rotated continuously when H is rotated in the bc plane.

independent of θ and the direction of $m_{\rm AFM}$ changes from the a to c axis continuously with increasing θ. This contradicts with the experimental results at $H = 5$ T where a discontinuous transition takes place at $\theta \sim 50°$ as shown in Fig. 9(b). Next, we consider the case where H is rotated in the bc plane above H^*. When $H \parallel c$ and b, $m_{\rm AFM}$ is parallel to the a and c axes, respectively. When H is rotated in the bc plane, a discontinuous transition should take place in the intermediate θ region as shown in Fig. 18(b). However, the experimental results show that there does not exist such a transition in the bc plane. Thus, a spin-flop transition where $m_{\rm AFM}$ changes from the c to the a axis takes place at H^* is not consistent with the observed θ dependence of H^*. Next, we consider the case (II) in Fig. 18 where $m_{\rm AFM} \parallel b$ is realized above H^*. When H is rotated in the ca plane, a discontinuous transition should take place in the intermediate θ region because $m_{\rm AFM} \parallel b$ for $H \parallel c$ and $m_{\rm AFM} \parallel c$ for $H \parallel a$ as shown in Fig. 18(c). When H is rotated in the bc plane, $m_{\rm AFM}$ is always perpendicular to H independent of θ, and the direction of $m_{\rm AFM}$ changes from the b to c axis continuously. These are consistent with the observed θ dependence of H^* and are consistent with the results of our ^{27}Al NMR experiments.[31]

[1] V. M. Thiede, T. Ebel, and W. Jeitsschko, J. Mater. Chem. **8**, 125 (1998).
[2] A. I. Tursina, S. N. Nesterenko, E. V. Murashova, I. V. Chernyshev, H. Noel, and Y. D. Sropegin, Acta Crystallogr., Sect. E: Struct. Rep. Online **61**, i12 (2005).
[3] A. M. Strydom, Phys. B (Amsterdam) **404**, 2981 (2009).
[4] Y. Muro, K. Motoya, Y. Saiga, and T. Takabatake, J. Phys. Soc. Jpn. **78**, 083707 (2009).
[5] T. Nishioka, Y. Kawamura, T. Takesaka, R. Kobayashi, H. Kato, M. Matsumura, K. Kodama, K. Matsubayashi, and Y. Uwatoko, J. Phys. Soc. Jpn. **78**, 123705 (2009).
[6] M. Matsumura, Y. Kawamura, S. Edamoto, T. Takesaka, H. Kato, T. Nishioka, Y. Tokunaga, S. Kambe, and H. Yasuoka, J. Phys. Soc. Jpn. **78**, 123713 (2009).
[7] H. Tanida, D. Tanaka, M. Sera, C. Moriyoshi, Y. Kuroiwa, T. Takesaka, T. Nishioka, H. Kato, and M. Matsumura, J. Phys. Soc. Jpn. **79**, 043708 (2010).
[8] K. Hanzawa, J. Phys. Soc. Jpn. **79**, 043710 (2010).
[9] S. Kambe, H. Chudo, Y. Tokunaga, T. Koyama, H. Sasaki, T. U. Ito, K. Ninomiya, W. Higemoto, T. Takesaka, T. Nishioka, and Y. Miyake, J. Phys. Soc. Jpn. **79**, 053708 (2010).
[10] H. Tanida, D. Tanaka, M. Sera, C. Moriyoshi, Y. Kuroiwa, T. Takesaka, T. Nishioka, H. Kato, and M. Matsumura, J. Phys. Soc. Jpn. **79**, 063709 (2010).
[11] A. Kondo, J. Wang, K. Kindo, T. Takesaka, Y. Kawwamura, T. Nishioka, D. Tanaka, H. Tanida, and M. Sera, J. Phys. Soc. Jpn. **79**, 073709 (2010).
[12] H. Tanida, D. Tanaka, M. Sera, C. Moriyoshi, Y. Kuroiwa, T. Takesaka, T. Nishioka, H. Kato, and M. Matsumura, J. Phys. Soc. Jpn. **79**, 083701 (2010).
[13] Y. Muro, J. Kajino, K. Umeo, K. Nishimoto, R. Tamura, and T. Takabatake, Phys. Rev. B **81**, 214401 (2010).
[14] J. Robert, J.-M. Mignot, G. Andre, T. Nishioka, R. Kobayashi, M. Matsumura, H. Tanida, D. Tanaka, and M. Sera, Phys. Rev. B **82**, 100404 (2010).
[15] D. D. Khalyavin, A. D. Hillier, D. T. Adroja, A. M. Strydom, P. Manuel, L. C. Chapon, P. Peratheepan, K. Knight, P. Deen, C. Ritter, Y. Muro, and T. Takabatake, Phys. Rev. B **82**, 100405 (2010).
[16] D. T. Adroja, A. D. Hillier, P. P. Deen, A. M. Strydom, Y. Muro, J. Kajino, W. A. Kockelmann, T. Takabatake, V. K. Anand, J. R. Stewart, and J. Taylor, Phys. Rev. B **82**, 104405 (2010).
[17] J- M. Mignot, J. Robert, G. Andre, T. Nishioka, R. Kobayashi, M. Matsumura, H. Tanida, D. Tanaka, and M. Sera, J. Phys. Soc. Jpn. **80**, SA022 (2011).
[18] H. Kato, R. Kobayashi, T. Takesaka, T. Nishioka, M. Matsumura, K. Kaneko, and N. Metoki, J. Phys. Soc. Jpn. **80**, 073701 (2011).
[19] A. Kondo, J. Wang, K. Kindo, T. Takesaka, Y. Ogane, Y. Kawamura, T. Nishioka, D. Tanaka, H. Tanida, and M. Sera, J. Phys. Soc. Jpn. **80**, 013701 (2011).
[20] A. Kondo, J. Wang, K. Kindo, Y. Ogane, Y. Kawamura, S. Tanimoto, T. Nishioka, D. Tanaka, H. Tanida, and M. Sera, Phys. Rev. B **83**, 180415 (2011).
[21] Y. Muro, J. Kajino, T. Onimaru, and T. Takabatake, J. Phys. Soc. Jpn. **80**, SA021 (2011).
[22] K. Umeo, T. Ohsuka, Y. Muro, J. Kajino, and T. Takabatake, J. Phys. Soc. Jpn. **80**, 064709 (2011).
[23] K. Hanzawa, J. Phys. Soc. Jpn. **80**, 023707 (2011).
[24] H. Tanida, D. Tanaka, M. Sera, S. Tanimoto, T. Nishioka, M. Matsumura, M. Ogawa, C. Moriyoshi, Y. Kuroiwa, J. E. Kim, N. Tsuji, and M. Takata, Phys. Rev. B **84**, 115128 (2011).
[25] S. I. Kimura, T. Iizuka, H. Miyazaki, A. Irizawa, Y. Muro, and T. Takabatake, Phys. Rev. Lett. **106**, 056404 (2011).
[26] S. I. Kimura, Y. Muro, and T. Takabatake, J. Phys. Soc. Jpn. **80**, 033702 (2011).
[27] S. I. Kimura, T. Iizuka, H. Miyazaki, T. Hajiri, M. Matsunami, T. Mori, A. Irizawa, Y. Muro, J. Kajino, and T. Takabatake, Phys. Rev. B **84**, 165125 (2011).
[28] Y. Kawamura, S. Edamoto, T. Takesaka, T. Nishioka, H. Kato, M. Matsumura, Y. Tokunaga, S. Kambe, and H. Yasuoka, J. Phys. Soc. Jpn. **79**, 103701 (2010).
[29] H. Tanida, D. Tanaka, M. Sera, T. Nishoka, H. Kato, M. Matsumura, H. Harima, and H. Yasuoka, J. Phys. Soc. Jpn. **80**, 013708 (2011).
[30] M. Matsumura, H. Tanida, D. Tanaka, H. Kato, T. Nishioka, and M. Sera, J. Phys. Soc. Jpn. **80**, 085001 (2011).
[31] H. Tanida, D. Tanaka, Y. Nonaka, M. Sera, M. Matsumura, and T. Nishioka, Phys. Rev. B **84**, 233202 (2011).
[32] M. Ribault, J. Flouquet, P. Haen, F. Lapierre, J. M. Mignot, and F. Holtzberg, Phys. Rev. Lett. **45**, 1295 (1980).
[33] See, for example, J. G. Sereni, in *Handbook on the Physics and Chemistry of Rare Earths*, edited by K. A. Gschneider and L. Eyring (Elsevier, Amsterdam, 1991), Vol. 15, p. 1.
[34] Y. Kawamura, S. Tanimoto, T. Nishioka, H. Tanida, M. Sera, K. Matsubayashi, Y. Uwatoko, A. Kondo, K. Kindo, and C. Sekine, J. Phys.: Condens. Matter (to be published).
[35] M. Sera *et al*. (unpublished).
[36] M. Sera, S. Itabashi, and S. Kunii, J. Phys. Soc. Jpn. **66**, 1548 (1997).
[37] M. Sera, N. Sato, and T. Kasuya, J. Phys. Soc. Jpn. **57**, 1412 (1998).